Crystal structures of the DsbG disulfide isomerase reveal an unstable disulfide

Begoña Heras*, Melissa A. Edeling*, Horst J. Schirra*, Satish Raina†, and Jennifer L. Martin*‡

*Institute for Molecular Bioscience and Australian Research Council Special Research Centre for Functional and Applied Genomics, University of Queensland, Brisbane QLD 4072, Australia; and †Centre Médical Universitaire, Département de Biochimie Médicale, 1 Rue Michel-Servet, 1211 Geneva 4, Switzerland

Communicated by John Kuriyan, University of California, Berkeley, CA, April 20, 2004 (received for review February 25, 2004)

Dsb proteins control the formation and rearrangement of disulfide bonds during the folding of secreted and membrane proteins in bacteria. DsbG, a member of this family, has disulfide bond isomerase and chaperone activity. Here, we present two crystal structures of DsbG at 1.7- and 2.0-Å resolution that are meant to represent the reduced and oxidized forms, respectively. The oxidized structure, however, reveals a mixture of both redox forms, suggesting that oxidized DsbG is less stable than the reduced form. This trait would contribute to DsbG isomerase activity, which requires that the active-site Cys residues are kept reduced, regardless of the highly oxidative environment of the periplasm. We propose that a Thr residue that is conserved in the *cis*-Pro loop of DsbG and DsbC but not found in other Dsb proteins could play a role in this process. Also, the structure of DsbG reveals an unanticipated and surprising feature that may help define its specific role in oxidative protein folding. Thus, the dimensions and surface features of DsbG show a very large and charged binding surface that is consistent with interaction with globular protein substrates having charged surfaces. This finding suggests that, rather than catalyzing disulfide rearrangement in unfolded substrates, DsbG may preferentially act later in the folding process to catalyze disulfide rearrangement in folded or partially folded proteins.

A key step in the protein folding process is the formation of disulfide bonds between Cys residues. Organisms ranging from bacteria to humans have developed systems to control this oxidative process (1). The Dsb family of proteins catalyzes disulfide bond formation in bacteria through two distinct pathways, an oxidative and a reducing/isomerase pathway (2, 3). The DsbA–DsbB, or oxidative, pathway (4–6) introduces disulfide bonds into newly translocated proteins, but it can result in nonnative disulfide bonds. The DsbC/DsbG–DsbD, or isomerase, pathway (7–9) catalyzes the rearrangement of incorrect disulfide bonds, allowing proteins to fold correctly.

Despite important advances in this field, the mechanism of disulfide bond isomerization is poorly understood. Furthermore, it is not clear why two isomerases, DsbC and DsbG, are encoded in bacteria. The two proteins are related distantly, sharing only 24% sequence identity, and DsbG expresses at lower levels than DsbC. In addition, DsbG exhibits a more narrow substrate specificity than DsbC. Thus, it does not catalyze the classic redox protein reaction (insulin reduction), and unlike DsbC, it does not catalyze oxidative refolding of RNase (10).

We undertook structural studies of DsbG to shed light on its function and to identify reasons why two isomerases are encoded. The results provide evidence that, as with DsbA (11), the oxidized forms of DsbG and DsbC are less stable than their reduced forms, and they indicate that the two disulfide isomerases may recognize different protein targets.

Methods

Diffraction Data Measurement. Native and selenomethionine (SeMet)-labeled DsbG were produced and crystallized as described (12). Briefly, DsbG was oxidized before crystallization by addition of 1.7 mM (1,10-phenanthroline)copper(II). Crystals were obtained from 20% polyethylene glycol (PEG) 4000/0.1 M sodium citrate, pH 3.8–4/0.2 M ammonium sulfate. High-resolution and multiwavelength anomalous diffraction (MAD) data were collected at the Advanced Photon Source (Argonne National Laboratory, Argonne, IL). Native data for the reduced structure were measured from a dehydrated crystal ($0.2 \times 0.3 \times 0.05$ mm^3) at the BioCARS 14-BMC beamline, and MAD data were measured from a single dehydrated crystal ($0.1 \times 0.4 \times 0.05$ mm^3) at the 14-BMD beamline. Diffraction data were integrated and scaled by using DENZO and SCALEPACK (13).

Diffraction data for the mixed-redox DsbG crystal were measured by using an RU-H2R generator (copper wavelength, 1.542 Å; Rigaku, Tokyo) and an R-Axis IV^{++} detector with mirrors obtained from Osmic (Auburn Hills, MI). The crystal-to-detector distance was 150 mm, and the 2θ angle was 0°. The cooled-nitrogen stream was produced by using a CryoCool-LN2 (NFC-1259-XRD; CryoIndustries, Manchester, NH). Data were processed and scaled by using CRYSTALCLEAR 1.3 (Rigaku).

Structure Determination. The structure of reduced DsbG was solved by MAD phasing of the DsbG–selenomethionine (SeMet) derivative. Of the 18 possible selenium positions, 17 positions were in the asymmetric unit with the program SOLVE/RESOLVE (14). The resulting phases were used in the program ARP/WARP (15) for automated building of the protein structure. The structure was completed by manual building in program O (16). Refinement was performed by conjugate gradient minimization with a maximum-likelihood target in CNS (17) on the native 1.7-Å-resolution dataset.

Most of the structure was unambiguously assigned in the electron density map, and the final model accounts for 229 of the 231 encoded residues in each subunit (the N- and C-terminal residues 1 and 231 were not modeled). Residues 46–48 (the loop between strands β3 and β4) were difficult to model because of poor density, and one of these residues (Asp-47) has a disallowed main-chain conformation. Additionally, some surface residues have weak electron density and are modeled with reduced occupancies in the side chains (subunit A: Asp-22, Lys-28, Arg-78, Lys-95, and Lys-153; subunit B: Lys-28, Glu-35, Arg-78, Lys-95, Lys-153, Lys-168, Glu-180, Asn-198, and Lys-208). One of the two subunits in the asymmetric unit is modeled as reduced, and the other is modeled as a mixture of reduced (70%) and oxidized (30%) forms. The structure of DsbG solved from the rotating-anode data [both subunits are a mixture of reduced (30%) and oxidized (70%) forms] was solved by difference Fourier methods by using the structure of reduced DsbG. Refinement was performed by conjugate gradient minimization with a maximum-likelihood target in CNS (17) on the 2-Å-

Abbreviations: TRX, thioredoxin; MAD, multiwavelength anomalous diffraction.

Data deposition: The atomic coordinates and structure factors have been deposited in the Protein Data Bank, www.pdb.org (PDB ID codes 1V58 and 1V57 for reduced and mixed-redox DsbG, respectively).

‡To whom correspondence should be addressed at: Institute for Molecular Bioscience, University of Queensland, 306 Carmody Road, St. Lucia, Queensland 4072, Australia. E-mail: j.martin@imb.uq.edu.au.

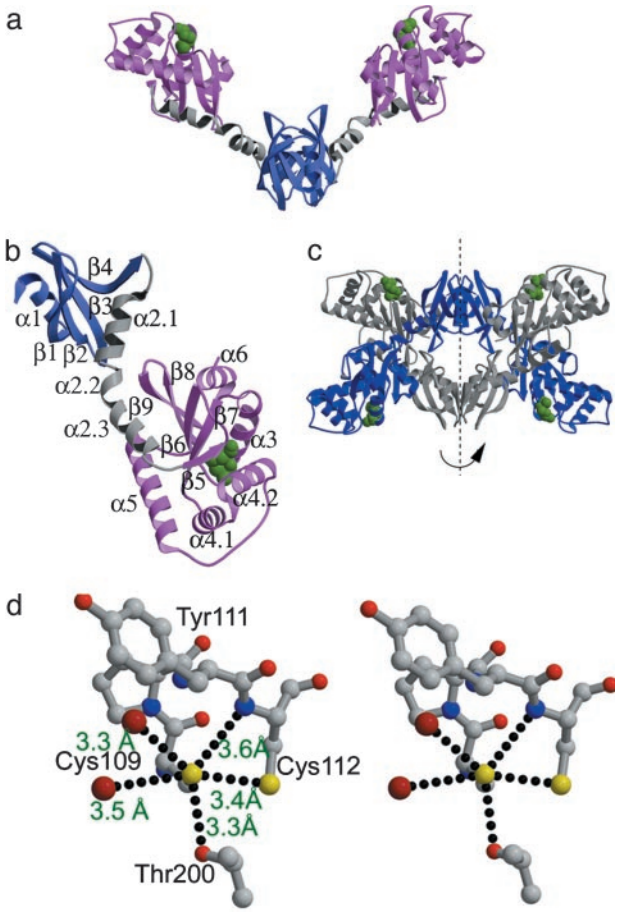

Fig. 1. Structure of DsbG. (*a*) Crystal structure of the DsbG homodimer. (*b*) Each DsbG monomer consists of an N-terminal dimerization domain (blue), a linker helix (gray), and a C-terminal catalytic domain that has a TRX fold (pink). The active-site disulfide is shown in green. (*c*) Interaction between the two V-shaped DsbG homodimers (blue and gray) found in the crystal structure. The asymmetric unit contains one blue subunit and one gray subunit. The biological dimer (two blue or two gray subunits) is generated by applying crystallographic symmetry, as indicated by an arrow. (*d*) Stereoview of interactions with the Cys at the active site of reduced DsbG (synchrotron data). Figures were generated with MOLSCRIPT (32).

resolution dataset. In the final structure, some surface residues with weak density were modeled with reduced occupancies for side-chain atoms (subunit A: Lys-28, Arg-78, Lys-94, Lys-95, and Lys-153; subunit B: Arg-78, Lys-95, Lys-153, Glu-180, Lys-208, and Glu-209).

Results

The crystal structure of DsbG at 1.7-Å resolution (Fig. 1 and Table 1) was determined by MAD. The two subunits in the asymmetric unit do not represent the biologically active dimer, which is instead formed from crystallographically related subunits (Fig. 1*c*). The two molecules in the asymmetric unit are a consequence of the interaction of two DsbG dimers (Fig. 1*c*).

The DsbG Fold. The N-terminal dimerization domain in each DsbG subunit (residues 1–61) has a cystatin-like fold found in cysteine protease inhibitors (18). The fold consists of an α-helix (α1), followed by a four-stranded antiparallel β-sheet (β1–β4) (Fig. 1*b*). The dimerization interface is formed by β-sheet interactions between the β4 strands of crystallographically related subunits.

The linker (residues 62–87) that connects the dimerization domain with the C-terminal catalytic domain comprises three sections forming a curved helix: α2.1 (residues 62–72), 3_{10}-helix α2.2 (residues 73–76), and helix α2.3 (residues 77–87) (Fig. 1*b*). This long linker places the two catalytic domains far apart and separates the N-terminal domain from the catalytic domain (Fig. 1*a*).

The catalytic domain (residues 88–231) incorporates a thioredoxin (TRX) fold (19) with a helical insert (α4, residues 136–177). As in all redox TRX-like proteins, a CXXC redox active center is located at the N terminus of the first helix (α3) (Fig. 1*b*).

DsbG Has an Unstable Disulfide. Crystals of DsbG were prepared from protein oxidized with copper phenanthroline (12), but the structure of DsbG revealed that the active-site Cys residues are reduced (Fig. 2*a*). The disulfide of DsbG is most likely reduced to the dithiol form in the crystal by the effects of the intense synchrotron radiation, as has been observed for other protein crystals (20). We, therefore, attempted to determine the structure of oxidized DsbG by using 2.0-Å-resolution data measured from crystals prepared and cryocooled in the same way but exposed to less intense X-radiation from a laboratory rotating-anode generator. The density for the side chains of the two Cys residues at the active site was continuous, indicating that the oxidized form was present, and the structure was, therefore, refined with a disulfide bond. The disulfide had the usual right-hand hook conformation (21) that is found in other TRX-fold redox proteins, and the bond length was close to ideal at 2.03 Å. Strong negative-difference density between the sulfur atoms (Fig. 2*b*), however, indicated that the disulfide bond did not represent the data adequately. The structure was then refined with a mixture of oxidized and reduced forms of the Cys residues. Different ratios of oxidized and reduced DsbG were tested, and the best model [which resulted in no difference density above noise level (2.5 σ) at the active site] was a mixture of 70% oxidized and 30% reduced DsbG (Fig. 2*b*).

The finding that the structure that was thought to be oxidized actually comprises a mixture of redox forms suggests that the disulfide bond of DsbG is unstable and that the equilibrium between the disulfide and dithiol forms strongly favors the reduced form. To investigate this finding further, we compared the structures of four Dsb proteins [the mixed-redox form of DsbG described here; oxidized DsbA (1DSB; 2.0-Å resolution; ref. 22); oxidized DsbC (1EEJ; 1.9-Å resolution; ref. 23); and oxidized CcmG (1KNG; 1.14-Å resolution; ref. 24)] to identify interactions specific to DsbG that might contribute to an unstable disulfide bond. The oxidized forms of all four structures revealed a short contact between the sulfur of the first Cys in the active-site CXXC motif and the main-chain nitrogen of the second Cys [DsbG, 3.1 Å; DsbA, 3.1 Å; DsbC, 3.0 Å; CcmG, 3.3 Å; expected range, 3.3–3.6 Å (25)]. In oxidized DsbG, however, there is another possible destabilizing interaction between Cys-109 Sγ and the side-chain hydroxyl of Thr-200 (3.5 Å; Fig. 3).

We wondered whether this interaction could be important for favoring reduced over oxidized DsbG. In TRX-like redox proteins such as DsbA and TRX, the residue at the equivalent position to Thr-200, immediately preceding the Pro in the *cis*-Pro loop, is hydrophobic: Val, Ala, or Ile. By contrast, in DsbGs and DsbCs, this residue is a conserved Thr (Fig. 4). However, if the disulfide of DsbG is less favored than the dithiol as a consequence of Thr-200, then DsbC should show the same effect. Discussions with the corresponding author of the DsbC crystal structure (23) (P. Metcalf, personal communication) indicated that difference density is present at the active site of DsbC; we, therefore, refined the structure of DsbC by using the deposited coordinates and structure factors (1EEJ; ref. 23) with different ratios of oxidized and reduced DsbC. As a control, we consid-

Table 1. Data collection and refinement statistics

	MAD (SeMet)			Native (synchrotron) reduced DsbG	Native (rotating anode) mixed-redox DsbG
	Peak	Inflection point	Remote		
Data collection					
Wavelength, Å	0.9783	0.9785	0.9556	0.9	1.5418
Resolution range, Å	100 to 2	100 to 2	100 to 2	26.5 to 1.7 (1.76 to 1.70)	32.2 to 2 (2.07 to 2.0)
a, Å	116.3	116.3	116.3	116.5	116.5
b, Å	57.0	57.0	57.0	57.2	57.0
c, Å	85.1	85.1	85.1	85.5	85.4
β, °	95	95	95	95	95
Space group	*C*2	*C*2	*C*2	*C*2	*C*2
Observed reflections	201,670	186,504	227,737	367,326	116,206
Unique reflections	64,522*	60,884*	69,469*	57,306	36,303
R_{merge}†‡	0.06 (0.14)	0.06 (0.15)	0.06 (0.14)	0.061 (0.269)	0.081 (0.31)
Completeness,‡ %	86.6 (34.3)	81.8 (23.3)	92.1 (49.3)	92.7 (53.5)	95.5 (88.0)
$\langle I\rangle/\langle\sigma(I)\rangle$‡	13.0 (4.1)	12.9 (3.6)	14.2 (6.0)	30.6 (3.9)	6.4 (2.1)
Phasing statistics					
Resolution, Å				100 to 2.0	
No. of selenium sites				17	
Mean figure of merit				0.42	
Refinement statistics					
No. of reflections in working set				55,837	36,299
No. of reflections in test set				5,688	3,621
R_{fac},§ %				18.6 (23.3)	19.9 (29.2)
R_{free},¶ %				20.7 (27.7)	23.2 (31.5)
No. of waters				550	549
Bonds,‖ Å				0.005	0.005
Angles,‖ °				1.30	1.2
Most favored regions,** %				93.8	92.8
Disallowed regions,** %				0.3	0.3
Average B factor, Å^2				28.1	28.1

SeMet, selenomethionine.
*Friedel pairs kept separate.
†$R_{merge} = \Sigma|I - \langle I\rangle|/\Sigma\langle I\rangle$, where I is the intensity of each individual reflection.
‡Values in parentheses refer to the highest resolution shell (1.70 to 1.81 Å for synchrotron data refinement and 2.0–2.13 Å for rotating anode refinement).
§$R_{fac} = \Sigma h|F_o - F_c|/\Sigma_i|F_o|$, where F_o and F_c are the observed and calculated structure-factor amplitudes for each reflection h.
¶R_{free} was calculated with 10% of the diffraction data selected randomly and excluded from refinement.
‖rms deviation from ideal geometry.
**Data from Ramachandran plot.

ered DsbA [1FVK; ref. 26; 1.7-Å resolution], which has a Val in place of the Thr.

For DsbC, negative difference density was found between the sulfur atoms in the CXXC active site, as we observed for DsbG (Fig. 2*c*). After refinement using a mixture of oxidized and reduced forms of the protein (monomer A: 50% oxidized, 50% reduced; monomer B: 75% oxidized, 25% reduced), no difference density was present above noise level (2.5 σ) between the two sulfur atoms (Fig. 2*c*). Furthermore, the Thr side chain from the *cis*-Pro loop of DsbC (Thr-182) is also 3.3–3.4 Å from the sulfur of the first Cys in the CXXC motif.

In the case of DsbA, no difference density was observed between the sulfur atoms of the disulfide (Fig. 2*d*), so the oxidized form adequately represents the measured data. These results support the hypothesis that a Thr at the *cis*-Pro loop of the active site (as found in DsbG and DsbC but not in other Dsb proteins) may favor the reduced state. In reduced DsbG, the Thr hydroxyl is within hydrogen bond distance of Cys-109 Sγ (3.3 Å; Figs. 1*d* and 3), whereas in DsbA structures, the Val is $\geq$3.8 Å from the equivalent sulfur. We prepared a DsbG mutant in which Thr-200 is replaced with Val, the residue type found at the same position in DsbA. This variant DsbG behaves very differently than native DsbG; expression levels were much lower compared with native or other DsbG mutants (data not shown); the crystals of oxidized DsbG T200V are extremely delicate (often dissolving when the crystallization trays are moved or when the cover slips are lifted) and have a different morphology to native crystals, and the diffraction resolution (2.7 Å) is much lower. At this resolution, it is difficult to determine unambiguously, however, the cysteines at the active site of DsbG T200V appear also to be a mixture of oxidized and reduced forms (data not shown). If this preliminary data is confirmed, it suggests that additional factors contribute to favoring the dithiol form of DsbG and DsbC.

Comparison of DsbG and DsbC Structures. The structure of DsbG resembles its distant homologue DsbC (24% sequence identity) (23). However, the dimensions of DsbG are significantly larger than those of DsbC (Fig. 4*a*), and the two protein structures cannot be superimposed directly because of the difference in length of the linker helix. The linker is 2.5 turns longer in DsbG compared with DsbC, and this extra length significantly alters the position of the catalytic domains relative to the dimerization domains.

The V-shaped cleft has been postulated as the binding site for unfolded proteins in DsbC (23). The different characteristics of the cleft in DsbG and DsbC, thereby, offer clues to

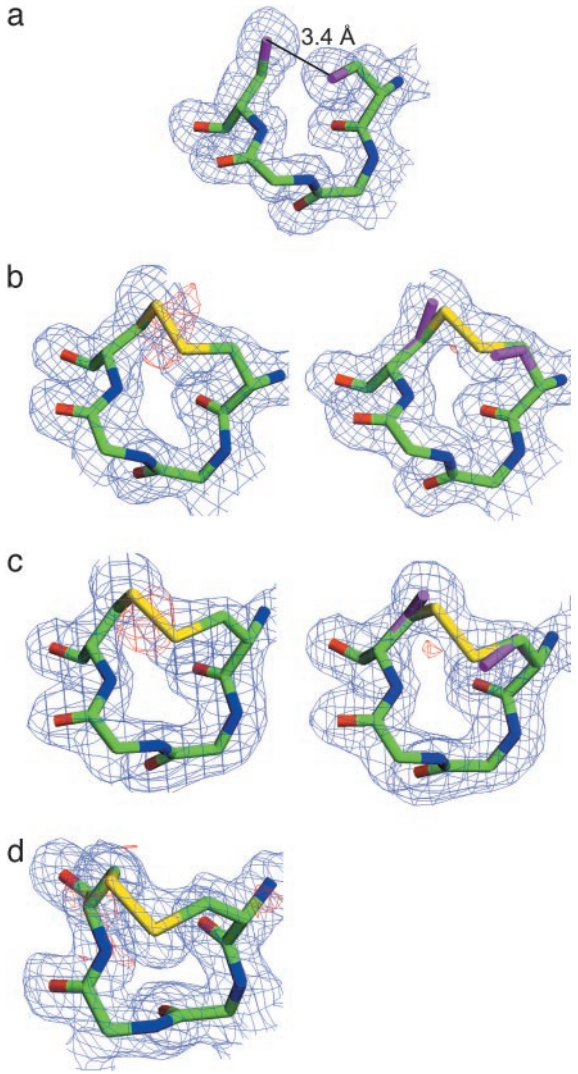

Fig. 2. Active-site residues $2F_o - F_c$ electron-density maps are shown at 1σ (blue), and $F_o - F_c$ electron-density maps are shown at -3σ (red). (*a*) Active site of reduced DsbG, with sulfur atoms shown in purple. (*b*) Active site of DsbG (rotating-anode data) before (*Left*) and after (*Right*) minimization with a mixture of 70% oxidized (yellow) and 30% reduced (purple) Cys. (*c*) Active site of oxidized DsbC (1EEJ) before (*Left*) and after (*Right*) minimization with a mixture of 50% oxidized (yellow) and 50% reduced (purple) Cys. (*d*) Active site of oxidized DsbA (FVK1). Electron-density representations were generated by using SETOR (33).

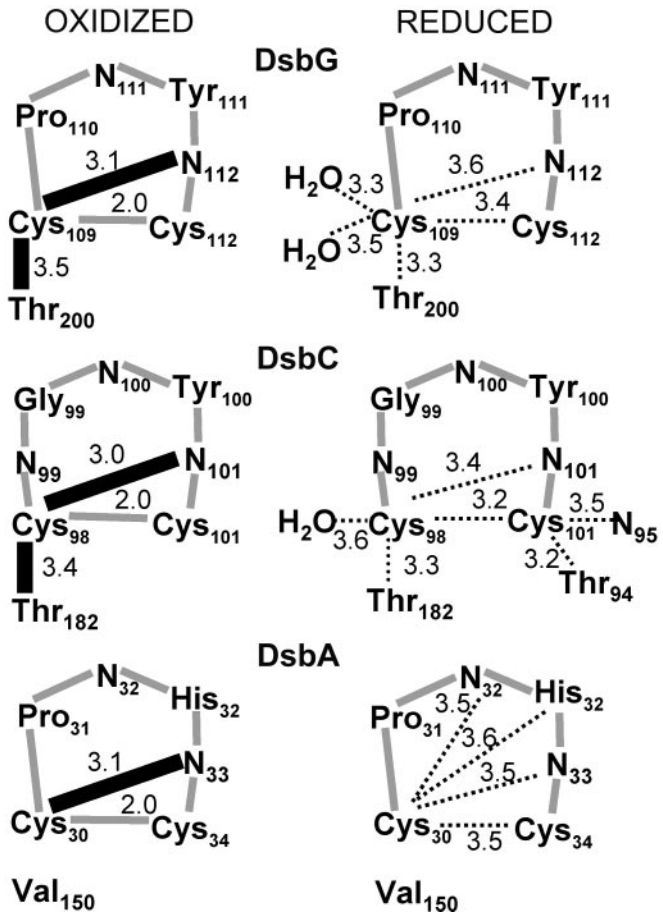

Fig. 3. Comparison of oxidized and reduced Dsb active sites by schematic representation showing interactions at the active sites of DsbG, DsbC, and DsbA in the oxidized and reduced forms. Covalent bonds (gray), hydrogen bonds (dotted line), and proposed destabilizing interactions (black) are shown. For comparison with the Thr interaction in the DsbG and DsbC structures, the position of Val-150 is indicated. However, the distance between Cys-30 of DsbA and Val-150 is 3.7–4.2 Å in oxidized DsbA and 4.5–4.6 Å in reduced DsbA.

their differing substrate specificity. The most obvious difference is the relative size, with the cleft in DsbG almost twice the size of that of DsbC (Fig. 4*a*). The other major difference is the surface charge. The inner surface of the DsbC cleft is lined with hydrophobic and uncharged residues. In contrast, DsbG has several acidic residues (Glu-11, Asp-36, Glu-69, Glu-79, Glu-189, Asp-193, and Asp-220) lining the cleft. These residues form negatively charged surface patches that are absent in DsbC (Fig. 4*b*) but are likely to be conserved in DsbGs (Fig. 4*c*). A third difference is a charged groove at the base of the "V" in DsbG, formed by residues in the loop connecting the $\beta 2$ and $\beta 3$ strands of the N-terminal domain. This loop is longer in DsbG than it is in DsbC, and the extra residues are polar and charged (Tyr-35, Gln-36, and Asp-37) (Fig. 4*b*). The insertion is highly conserved in DsbGs, suggesting that its function is also conserved.

Discussion

The TRX fold is the core scaffold in proteins with very different functions (19). Among them, the TRX-like oxidoreductases (including TRX and Dsb proteins) control the cellular redox environment, which is critical for the folding and stability of other proteins (1–3). The TRX-like redox proteins share no overall sequence homology, yet they all contain a CXXC motif and a *cis*-Pro loop at the active site.

The crystal structures of DsbG reveal that its disulfide bond is sensitive to synchrotron radiation. This result alone is not novel in that disulfides in other protein structures also have been reduced by synchrotron radiation (20). However, disulfides in frozen protein crystals are generally resistant to rotating-anode radiation. In an attempt to prevent disulfide reduction in DsbG crystals, data were, therefore, measured from a frozen DsbG crystal on a rotating-anode x-ray source. However, this treatment did not resolve the problem because the structure revealed a mixture of oxidized (70%) and reduced (30%) DsbG. The mixture of redox forms in DsbG is likely to be a combination of incomplete oxidation by copper phenanthroline (data not shown) and high sensitivity to radiation-induced disulfide reduction.

The crystal structure data for DsbG, DsbC, and DsbA correlate well with thermodynamic data on their thiol disulfide

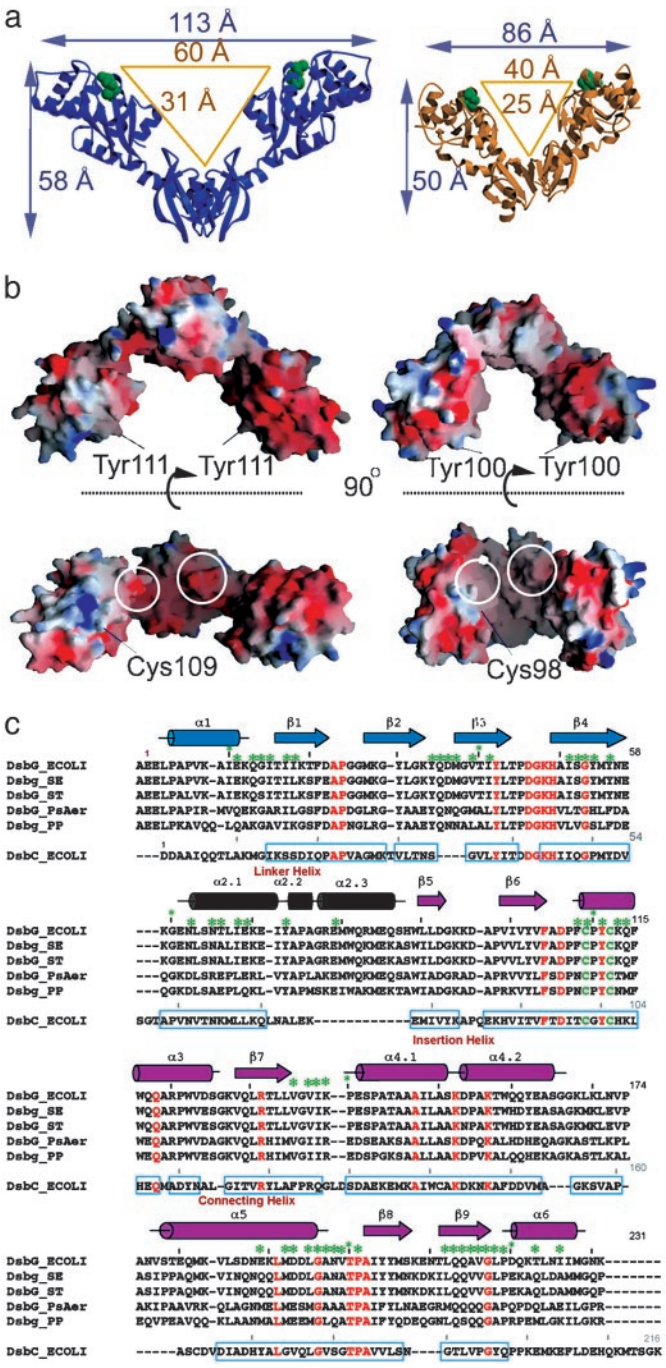

Fig. 4. Comparison of DsbG and DsbC. (*a*) Dimensions of DsbG (blue) and DsbC (yellow). (*b*) Surface representation of DsbG (*Left*) and DsbC (*Right*) in two different orientations (*Upper* and *Lower*) related by a 90° rotation along the *x* axis. Positive and negative electrostatic potentials are shown in blue and red, respectively (saturation, 15 kT/e). Circles indicate regions of the surface that are charged in DsbG but uncharged in the hydrophobic cleft of DsbC. Electrostatic surface representations were generated by using GRASP (34). (c) Multiple sequence alignment of DsbG homologs obtained from a search of the Swissprot/Trembl database (January 2003). DsbG_ECOLI, *Escherichia coli* DsbG; DsbG_ST, *Salmonella enterica* DsbG; DsbG_SE, *Salmonella typhimurium* DsbG; DsbG_PsAer, *Pseudomonas aeruginosa* DsbG; DsbG_PP, *Pseudomonas putida* DsbG; and DsbC_ECOLI, *Escherichia coli* DsbC. Identical residues are shown in red, and the two active-site Cys residues in each sequence are shown in green. Secondary structure elements are based on the DsbG_ECOLI structure. Boxes indicate regions of DsbG that can be aligned structurally (as independent domains) with DsbC. Residues that line the V-shaped cleft are indicated by green asterisks.

equilibrium (7, 10, 11, 27, 28). In all three proteins, the redox potentials indicate that the reduced form is favored over the oxidized form. DsbA is the most oxidizing protein with a redox potential of −119 mV (11). Its high redox potential arises from a very low pK_a (≈3.5) for the solvent-accessible Cys (Cys-30). The thiolate anion of Cys-30 is stabilized by interactions with His-32 in the Cys-30-Pro-31-His-32-Cys-33 active site and by several other hydrogen bonds (29) (Fig. 3). DsbC has a redox potential of −130 mV (7) and DsbG has a similar redox potential [values reported are −126 mV (10) and −129mV (28)]. The redox potentials for DsbG and DsbC indicate that the reduced form is more favored than the respective oxidized form of the protein but not as favored as the reduced form of DsbA. We propose that this difference is because neither DsbG (Cys-Pro-Tyr-Cys) nor DsbC (Cys-Gly-Tyr-Cys) has a His at the active site, which is critical for stabilizing the reduced form of DsbA. However, these proteins both have a Thr in the *cis*-Pro loop, and this residue favors the reduced form of the protein by interaction with the sulfur of the first Cys in the active site (Fig. 3). Furthermore, in the oxidized forms of DsbG and DsbC the Thr side chain maintains close contact with the sulfur (Fig. 3), unlike the His side chain in DsbA, which moves 2–3 Å away in the oxidized form. The close association of the Thr side chain to the Cys sulfur in oxidized DsbG could destabilize the disulfide kinetically by providing a proton donor to facilitate reduction. Additional hydrogen bonds between the cysteines and water molecules (DsbG) or a second Thr side chain (DsbC) (Fig. 3) could also favor the reduced form over the oxidized form.

It is also interesting to note the recent work of Kakodura *et al.* (30) on mutations in the *cis*-Pro loop of DsbA (G-V-*cis*P) that dramatically affect activity. They found that a P151T mutant in which the *cis*-Pro is replaced with Thr accumulates DsbA–substrate complexes. This result indicates that resolution of the DsbA–substrate complexes is retarded, and the authors postulate that the *cis*-Pro ring may be important for maintaining correct positioning of the DsbA–substrate disulfide bond. However, a P151S mutation has a different phenotype, suggesting that removal of the Pro ring does not explain the effect of the P151T mutation fully. Our results suggest that it may be the Thr side chain specifically, rather than the lack of a Pro, that is significant. It will, therefore, be interesting to investigate the function of DsbA V150T, in which the Val of DsbA is replaced by a Thr as in DsbG and DsbC and the *cis*-Pro is unchanged. In DsbG and DsbC, the conserved Thr may facilitate isomerization activity in the same way that the DsbA mutant is thought to trap substrate complexes by increasing the resolution time of the mixed disulfide bond with the target protein. Slowing down this specific step in the redox reaction could favor the formation of correct disulfide bonds.

What is the precise function of DsbG, and which are its target substrates? Bessette *et al.* (10) reported that overexpression of *dsbG* can partially rescue the formation of multidisulfide proteins in a *dsbC* mutant background. They also found that DsbG is inactive in the classic insulin-reduction assay. This result and more recent results (31) lead to the conclusion that DsbG acts as a thiol/disulfide isomerase with a narrower substrate specificity than DsbC. We investigated structural differences at the binding cleft of DsbG and DsbC to identify features that could give clues to substrate specificity. We found the following important differences. (*i*) DsbG has a significantly longer helical linker than DsbC, which substantially increases the dimensions of the binding-site cleft, (*ii*) conserved acidic residues in DsbG form negatively charged patches in the otherwise hydrophobic cleft and these are not present in DsbC, and (*iii*) a longer loop between strands $\beta 2$ and $\beta 3$ of DsbG forms a groove incorporating conserved polar/charged residues at the base of the hydrophobic cleft.

These differences between DsbG and DsbC suggest that the two proteins interact with considerably different substrates. The uncharged surface of DsbC is consistent with it interacting with unfolded proteins because these substrates would expose hydrophobic residues on their surface. However, the size and surface charge of the DsbG binding sites indicates that its substrates are likely to be much larger than those of DsbC and that they could have charged surfaces. Target proteins of DsbG could be at least as large as DsbG itself, as indicated by crystal packing (Fig. 1*c*). The characteristics of the DsbG binding surface (large with charged surface) are consistent with binding target proteins that are folded or partially folded. Thus, the isomerase function of DsbG may be directed at proteins that are further along the folding pathway than those that interact with DsbC. This finding would also help to explain why two disulfide bond isomerases are encoded in bacteria.

We thank Harry Tong, Christine L. Gee, and Fiona M. McMillan for assistance with data collection; Peter Metcalf for helpful discussions; and the Advanced Photon Source (Argonne National Laboratory) for the use of facilities. J.L.M. was supported by grants from the Australian Synchrotron Research Program, an Australian Research Council grant, and an Australian Research Council Senior Research Fellowship. H.J.S. was supported by an Australian Research Council Postdoctoral Fellowship.

1. Debarbieux, L. & Beckwith, J. (1999) *Cell* **99**, 117–119.
2. Collet, J. F. & Bardwell, J. C. (2002) *Mol. Microbiol.* **44**, 1–8.
3. Kadokura, H., Katzen, F. & Beckwith, J. (2003) *Annu. Rev. Biochem.* **72**, 111–135.
4. Bardwell, J. C., McGovern, K. & Beckwith, J. (1991) *Cell* **67,** 581–589.
5. Bardwell, J. C., Lee, J. O., Jander, G., Martin, N., Belin, D. & Beckwith, J. (1993) *Proc. Natl. Acad. Sci. USA* **90,** 1038–1042.
6. Guilhot, C., Jander, G., Martin, N. L. & Beckwith, J. (1995) *Proc. Natl. Acad. Sci. USA* **92,** 9895–9899.
7. Zapun, A., Missiakas, D., Raina, S. & Creighton, T. E. (1995) *Biochemistry* **34,** 5075–5089.
8. Missiakas, D., Schwager, F. & Raina, S. (1995) *EMBO J.* **14,** 3415–3424.
9. Rietsch, A., Belin, D., Martin, N. & Beckwith, J. (1996) *Proc. Natl. Acad. Sci. USA* **93,** 13048–13053.
10. Bessette, P. H., Cotto, J. J., Gilbert, H. F. & Georgiou, G. (1999) *J. Biol. Chem.* **274,** 7784–7792.
11. Zapun, A., Bardwell, J. C. & Creighton, T. E. (1993) *Biochemistry* **32**, 5083–5092.
12. Heras, B., Edeling, M. A., Byriel, K. A., Jones, A., Raina, S. & Martin, J. L. (2003) *Structure (London)* **11**, 139–145.
13. Otwinowski, Z. & Minor, W. (1997) *Methods Enzymol.* **276**, 307–326.
14. Terwilliger, T. C. & Berendzen, J. (1999) *Acta Crystallogr. D* **55**, 849–861.
15. Perrakis, A., Morris, R. J. & Lamzin, V. S. (1999) *Nat. Struct. Biol.* **6**, 458–463.
16. Jones, T., Zou, J. Y., Cowan, S. W. & Kjeldgaard, M. (1991) *Acta Crystallogr. A* **47**, 110–119.
17. Brunger, A. T., Adams, P. D., Clore, G. M., DeLano, W. L., Gros, P., Grosse-Kunstleve, R. W., Jiang, J. S., Kuszewski, J., Nilges, M., Pannu, N. S., *et al.* (1998) *Acta Crystallogr. D* **54**, 905–921.
18. Bode, W., Engh, R., Musil, D., Thiele, U., Huber, R., Karshikov, A., Brzin, J., Kos, J. & Turk, V. (1988) *EMBO J.* **7**, 2593–2599.
19. Martin, J. L. (1995) *Structure (London)* **3,** 245–250.
20. Schroder Leiros, H. K., McSweeney, S. M. & Smalas, A. O. (2001) *Acta Crystallogr. D* **57**, 488–497.
21. Hutchinson, E. G. & Thornton, J. M. (1996) *Protein Sci.* **5**, 212–220.
22. Martin, J. L., Bardwell, J. C. & Kuriyan, J. (1993) *Nature* **365**, 464–468.
23. McCarthy, A. A., Haebel, P. W., Torronen, A., Rybin, V., Baker, E. N. & Metcalf, P. (2000) *Nat. Struct. Biol.* **7**, 196–199.
24. Edeling, M. A., Guddat, L. W., Fabianek, R. A., Thöny-Meyer, L. & Martin, J. L. (2002) *Structure (London)* **10**, 973–979.
25. Gregoret, L. M., Rader, S. D., Fletterick, R. J. & Cohen, F. E. (1991) *Proteins* **9**, 99–107.
26. Guddat, L. W., Bardwell, J. C., Zander, T., Martin, J. L. (1997) *Protein Sci.* **6**, 1148–1156.
27. Huber-Wunderlich, M. & Glockshuber, R. (1998) *Folding Des.* **3**, 161–171.
28. van Straaten, M., Missiakas, D., Raina, S. & Darby, N. J. (1998) *FEBS Lett.* **428**, 255–258.
29. Guddat, L. W., Bardwell, J. C. & Martin, J. L. (1998) *Structure (London)* **6**, 757–767.
30. Kadokura, H., Tian, H., Zander, T., Bardwell, J. C. A. & Beckwith, J. (2004) *Science* **303**, 534–537.
31. Hiniker, A. & Bardwell, J. C. (2004) *J. Biol. Chem.* **279,** 12967–12973.
32. Kraulis, P. J. (1991) *J. Appl. Crystallogr.* **24,** 946–950.
33. Evans, S. V. (1993) *J. Mol. Graphics* **11,** 134–138.
34. Nicholls, A., Sharp, K. & Honig, B. (1991) *Proteins* **11**, 281–296.